Astron. Astrophys. 319, 995–1006 (1997)

ASTRONOMY
AND
ASTROPHYSICS

A 2 1/2 D thermodynamic model of cometary nuclei

I. Application to the activity of comet 29P/Schwassmann-Wachmann 1

A. Enzian, H. Cabot, and J. Klinger

Laboratoire de Glaciologie et Géophysique de l'Environnement du CNRS, Université Joseph Fourier, Grenoble I, B.P. 96, 54 Rue Molière, F-38402 St Martin d'Hères, France

Received 27 June 1996 / Accepted 5 September 1996

Abstract. A $2\frac{1}{2}$ dimensional model of cometary nuclei is presented. The comet is considered as a porous ice-dust medium. Heat and gas diffusion between the surface and the inner part of the nucleus is considered. Going beyond models published so far, this work takes into account nucleus rotation and a two dimensional resolution of the diffusion equations, including a gas diffusion theory derived from the Boltzmann equation. The icy constituent is considered to be initially amorphous water ice containing solid carbon monoxide. The crystallisation of the amorphous ice follows an activation law found by means of laboratory studies.

The model is applied to comet 29P/Schwassmann-Wachmann 1. This comet is of particular interest due to its strong activity and its unpredictable outbursts. We consider that the activity is driven by a sublimation process taking place below the nucleus surface. Special attention is given to the obliquity of the rotation axis. The model results are in good agreement with observed gas and dust production rates. It was in particular possible to produce outbursts of activity as they are observed for this comet. The best fit of the observation is obtained for a nucleus containing initially amorphous ice and having a tilted rotation axis. The surface erosion, considered to be very small so far for comet 29P/Schwassmann-Wachmann 1, is necessary to maintain an outburst regime due to crystallisation. No irregularities in its activity were found in runs where the model nucleus contained crystalline water ice with carbon monoxide. Thus, this work is an important clue for the presence of amorphous water ice in cometary nuclei.

Key words: comets: 29P/Schwassmann-Wachmann 1 – conduction – diffusion – comets: general – methods: numerical

1. Introduction

Periodic comet Schwassmann-Wachmann 1 (hereafter referred to as P/SW1) is known for its irregular lightcurve. Compared to other comets, its orbit has only a very small eccentricity (present state e = 0.045). Its mean heliocentric distance is about 6 AU. Although most other comets observed at this distance appear as faint objects P/SW1 has a persistent coma throughout its orbit and a strong unpredictable variability of its brightness is reported (Whipple 1980). In recent data analyses Cabot et al. (1996) and Cabot (1996) found a correlation between the mean brightness and the heliocentric distance. It was only during the last few years that carbon monoxide (CO) could be identified by means of radio spectroscopic observations as an important driver of the activity of P/SW1. Indeed, this molecule has already been suspected as free water ice sublimation is too weak at 6 AU to account for the observed brightness. The derived CO production rate is $2\,10^{28}$ - $5\,10^{28}$ molecules s^{-1} (Senay & Jewitt 1994; Crovisier et al. 1995) which seems to be more or less stable since more recent observations come up with similar values. During an outburst, however, increases of a factor 4 have recently been observed (Bockelée-Morvan, private communication). The CO production rate is sufficient to generate the observed coma.

In this study we investigate the activity of P/SW1 by means of numerical modelling. We present a thermodynamic model of cometary nuclei. Its development is motivated in part by the need of a working model for the future Rosetta mission. The model concept is akin to earlier works (e.g. Espinasse et al. 1989, 1991; Tancredi et al. 1994). The main achievement of this model is a high spatial and temporal resolution as well as a physically more fundamental description of the gas diffusion within the nucleus. In fact, comet nucleus models published so far have typically used the *fast rotator* approximation of a sphere. Transport equations for heat and gas are numerically integrated exclusively for the radial direction with a time step of a few days. Unlike the *fast rotator* approximation, physico-chemical reactions taking place in comets are non-linear with respect to temperature and can be very different at the poles and the equator as well as between day and night. The transport equations in our model are integrated for the radial and meridional directions. A 3D solution is obtained by relating the boundary conditions to the comet's hour angle. For simplification several of the previous models assume that only Knudsen gas diffusion takes place inside the nucleus

Send offprint requests to: A. Enzian

(e.g. Benkhoff 1995; Tancredi et al. 1994). Some works seek a more complete description by using parametrised diffusion coefficients of a free molecular and a viscous regime (e.g. Fanale & Salvail 1984; Prialnik et al. 1990). Other works studied also the transition of a gas from a molecular to a viscous regime (e.g. Steiner 1991; Bouziani 1995). In this work we adapted the *Chapman-Enskog* method (Chapman & Cowling 1960) which has not been used so far for cometary modelling. This method provides transport coefficients of pure or mixed gases for all possible diffusion regimes from the solution of the linearised Boltzmann equation.

We consider that with these new achievements the model provides production rates which can be directly tested against those measured by astronomical observations.

2. Model description

2.1. Composition

The model nucleus is composed of fluffy ice-dust aggregates. These aggregates are supposed to have a similar fractal dimension (see Eq. 55). The dust component stands for a non-volatile phase with a low visible albedo. The icy constituent is composed of carbon monoxide enriched water ice which is initially in the amorphous state. Some amount of the condensed CO may evaporate by temperature controlled sublimation. However, as shown by Schmitt et al. (1989), a small fraction is trapped by the amorphous ice and can only escape during the crystallisation of the amorphous matrix. We consider that amorphous and crystalline water ice can coexist before complete crystallisation. The composition of the solid ice-dust matrix is described by the mass concentration of each constituent. We use $\tilde{\rho}_d$ for the mass of dust per unit volume, $\tilde{\rho}_{\mathrm{H_2O}}$ for the water ice concentration and $\tilde{\rho}_{\mathrm{CO}}$ for the concentration of solid carbon monoxide. We will later also use $\tilde{\rho}^a_{\mathrm{H_2O}}$ and $\tilde{\rho}^c_{\mathrm{H_2O}}$ ($\tilde{\rho}_{\mathrm{H_2O}} = \tilde{\rho}^a_{\mathrm{H_2O}} + \tilde{\rho}^c_{\mathrm{H_2O}}$) to distinguish between amorphous and crystalline ice. Additionally we denote $\tilde{\rho}^t_{\mathrm{CO}}$ and $\tilde{\rho}^f_{\mathrm{CO}}$ ($\tilde{\rho}_{\mathrm{CO}} = \tilde{\rho}^t_{\mathrm{CO}} + \tilde{\rho}^f_{\mathrm{CO}}$) for the concentrations of trapped and free CO. The mass density of the matrix can then be written as

$$\rho = \tilde{\rho}_d + \tilde{\rho}_{\mathrm{H_2O}} + \tilde{\rho}_{\mathrm{CO}} \tag{1}$$

The porosity, which is here defined as the ratio of the pore volume to total volume of the matrix, is given by comparing the mass concentration of each constituent with the density of a compact solid (ρ_d, $\rho_{\mathrm{H_2O}}$, ρ_{CO}).

$$po = 1 - \frac{\tilde{\rho}_d}{\rho_d} - \frac{\tilde{\rho}_{\mathrm{H_2O}}}{\rho_{\mathrm{H_2O}}} - \frac{\tilde{\rho}_{\mathrm{CO}}}{\rho_{\mathrm{CO}}} \tag{2}$$

The amount of trapped CO is supposed in the model to be directly related to the amorphous ice aggregate. The CO mass concentration is proportional to the mass concentration of H_2O.

$$\tilde{\rho}^t_{\mathrm{CO}} = f_t\, \tilde{\rho}^a_{\mathrm{H_2O}} \tag{3}$$

The dust to ice mass ratio of the solid matrix is given by

$$\psi = \frac{\tilde{\rho}_d}{\tilde{\rho}_{\mathrm{H_2O}} + \tilde{\rho}_{\mathrm{CO}}} \tag{4}$$

At the beginning of the simulation the model nucleus has a uniform composition.

2.2. Physico-chemical reactions

Below the surface the material is initially in thermodynamic equilibrium. A small temperature rise induces sublimation. The statistical sublimation (or condensation) rate of a species i ($\dot{Q}^{st}_i$) can be estimated using the kinetic gas theory.

$$\dot{Q}^{st}_i = \mathscr{S} \cdot \alpha \, \frac{p^s_i - p_i}{\sqrt{2\pi m_i k_B T}} \tag{5}$$

($i \equiv \mathrm{H_2O}$, CO). This expression holds for the sublimation rate within a unit volume. T stands for the temperature which is supposed to be identical in the gas and in the solid phase. k_B is the Boltzmann constant and m_i represents the molecular mass of species i. The saturated vapour pressure p^s_i and the partial pressure p_i are corrected by the sticking (or condensation) coefficient α. $\mathscr{S}$ is the volume specific surface. It can be shown that the characteristic time scale of sublimation is much shorter than those of heat and gas diffusion (e.g. Tancredi et al. 1994). Hence, the gas should be close to saturation if sufficient ice is present. Significant deviation from saturation can exist within the first few centimetres beneath surface. This effect has been confirmed by means of laboratory experiments (Kömle et al. 1992). Saturation is reached if $p_i = p^s_i$. We introduce a phenomenological description of the sublimated gas per unit volume during a given time interval

$$\frac{\Delta Q^{ph}_i}{\Delta t} = po \, \left(p^s_i - p_i\right) / \Delta t \tag{6}$$

This leads to an enthalpy change due to sublimation of

$$\Delta H^s_i = L^s_i \, \frac{m_i}{k_B T} \, \Delta Q^{ph}_i \tag{7}$$

where L^s_i is the latent heat of sublimation.

The crystallisation rate is determined using the time scale for complete crystallisation found by Schmitt et al. (1989).

$$\frac{\partial \tilde{\rho}^a_{\mathrm{H_2O}}}{\partial t} = 1.05\, 10^{13}\ \mathrm{s}^{-1} \ \exp\left(\frac{-5370\ \mathrm{K}}{T}\right) \tilde{\rho}^a_{\mathrm{H_2O}} \tag{8}$$

This time scale has been found by analysing the time evolution of the shape and position of both the 3.1 and 6.0 μm infrared absorption bands of H_2O in pure and gas enriched water ice. The crystallisation of amorphous water ice is an irreversible exothermic process. This process starts by forming a cubic lattice. In a following stage cubic ice transforms to hexagonal ice. The enthalpy change during the last phase transition is small compared to the first one. Amorphous water ice has a particularly large specific surface area which plays an important role for the adsorption of very volatile molecules like CO. When the amorphous ice matrix is heated, molecules being adsorbed in deep sites can be trapped due to surface rearrangements. The evaporation rate of CO during crystallisation is given for a constant release by

$$\dot{Q}^{cr}_{\mathrm{CO}} = f_t \, \frac{k_B T}{m_{\mathrm{H_2O}}} \frac{\partial \tilde{\rho}^a_{\mathrm{H_2O}}}{\partial t} \tag{9}$$

The net enthalpy change of this process has to account for the latent heat of crystallisation and the evaporation energy of trapped CO.

$$\dot{H}^{cr} = \left(L^{cr}_{\mathrm{H_2O}} - f_t\, L^{ev}_{\mathrm{CO}}\right) \frac{\partial \tilde{\rho}^{a}_{\mathrm{H_2O}}}{\partial t} \tag{10}$$

2.3. Diffusion equations

The transport of heat and gas is defined by means of a system of three coupled diffusion equations.

$$\rho c_p \frac{\partial T}{\partial t} = \nabla\left(K\,\nabla T\right) + \sum \dot{H} \tag{11}$$

$$\frac{\partial p_i}{\partial t} = \nabla(\underbrace{D^d_i\,\nabla p_i}_{\textit{diffusive}}) + \nabla(\underbrace{D^v_i\,\nabla p}_{\textit{viscous}}) + \sum \dot{Q}_i \tag{12}$$

K stands for the effective thermal conductivity of the solid matrix. Additional heat sources (sublimation, crystallisation and advection) are represented by a source term $\sum \dot{H}$. The gas diffusion equations apply to viscous, free molecular (or Knudsen) and mutual (or Fick) diffusion. p_i is the partial pressure of species i and $p = p_i + p_j$ is the total gas pressure of a binary gas mixture. D^d_i and D^v_i are the diffusion coefficients for diffusive and viscous flow. Additional gas sources are denoted with $\sum \dot{Q}_i$.

The thermal conductivity of cometary material is unknown so far. One can expect that its value is very sensitive to structure parameters of the porous matrix which may change during the comet's thermodynamic evolution. We use a parametrised expression for the effective thermal conductivity. As an upper limit of the conduction we use a parallel network.

$$K = h\left(\frac{\tilde{\rho}^{c}_{\mathrm{H_2O}}}{\rho^{c}_{\mathrm{H_2O}}} K^{c}_{\mathrm{H_2O}} + \frac{\tilde{\rho}^{a}_{\mathrm{H_2O}}}{\rho^{a}_{\mathrm{H_2O}}} K^{a}_{\mathrm{H_2O}} + \frac{\tilde{\rho}_{\mathrm{CO}}}{\rho_{\mathrm{CO}}} K_{\mathrm{CO}} + \frac{\tilde{\rho}_d}{\rho_d} K_d\right) + 4 r_p \epsilon \sigma T^3 \tag{13}$$

The parameter h is generally called hertz factor. Throughout one simulation we use a constant value for h. The last term of Eq. (13) accounts for the heat transport by means of infrared radiation, where r_p is a characteristic pore size, ϵ is the infrared emissivity and σ is the Stefan-Boltzmann constant.

The gas diffusion coefficients are adopted from the *Chapman-Enskog* method (Chapman & Cowling 1960). For a binary gas mixture the coefficients are

$$D^d_i = D_i\left(1 - \chi_i \delta_i \beta_i\right)^{-1} \tag{14}$$

$$D^v_i = \chi_i \left[\delta_i D_{mj} + \left(\delta_i \frac{D_{mj}}{\tilde{D}_m} + 1 - \delta_i\right) \frac{\xi \pi r_p^4 p}{8 \eta_{ij}}\right] \cdot \left(1 - \chi_i \delta_i \beta_i\right)^{-1} \tag{15}$$

where χ_i is the molar fraction of species i. ξ is a geometrical parameter describing the ratio of the gas flux across a porous material to the gas flux in a capillary of radius r_p. This parameter will be discussed more in detail at the end of this section. β_i is given by

$$\beta_i \approx 1 - \left(\frac{m_i}{m_j}\right)^{1/2} \tag{16}$$

m_i and m_j are the molecular masses of species i and j. δ_i expresses the ratio of the unreduced diffusive diffusion coefficient D_i to the mutual diffusion coefficient D_{ij}.

$$\delta_i = \frac{D_i}{D_{ij}} \tag{17}$$

D_i is defined by

$$D_i^{-1} = D_{ij}^{-1} + D_{mi}^{-1} \tag{18}$$

D_{mi} is the free molecular diffusion coefficient. $\tilde{D}_m^{-1}$ is given by

$$\tilde{D}_m^{-1} = \frac{\chi_i}{D_{mi}} + \frac{\chi_j}{D_{mj}} \tag{19}$$

The viscosity η_{ij} for a binary gas mixture is given by

$$\eta_{ij} = \frac{\frac{5\pi}{32} m_i \bar{v}_i \left(\sqrt{2}\pi d_i^2\right)^{-1}}{1 + \frac{p_j}{p_i}\left(\frac{d_{ij}}{d_i}\right)^2 \sqrt{\frac{m_i + m_j}{2m_i}}} + \frac{\frac{5\pi}{32} m_j \bar{v}_j \left(\sqrt{2}\pi d_j^2\right)^{-1}}{1 + \frac{p_i}{p_j}\left(\frac{d_{ij}}{d_j}\right)^2 \sqrt{\frac{m_i + m_j}{2m_j}}} \tag{20}$$

where $d_{ij} = \frac{1}{2}(d_i + d_j)$. d_i and d_j are the diameters of the molecules treated as rigid elastic spheres. The mutual diffusion coefficient is (e.g. Present 1958)

$$D_{ij} = \frac{3}{8}\left(\frac{\pi k_B T}{2m^*}\right)^{\frac{1}{2}} \frac{k_B T}{p \pi d_{ij}^2} \tag{21}$$

where $m^* = \frac{m_i m_j}{m_i + m_j}$ is the reduced mass. The free molecular diffusion coefficient inside a disordered porous medium is strongly dependent on the interfacial geometry and the connectivity of the pore network. Following Levitz (1993) (see also Dullien 1992) we introduce

$$D_{mi} = \frac{1}{3} \frac{\langle \ell_p \rangle \langle v_i \rangle}{\tau} \tag{22}$$

where $\langle v \rangle$ is the mean thermal gas velocity.

$$\langle v_i \rangle \approx \bar{v}_i = \sqrt{\frac{8 k_B T}{\pi m_i}} \tag{23}$$

The random walk of gas molecules is considered by a succession of chords belonging to the pore network. One chord begins and ends at a solid surface. For a random packing of hard spheres the mean free path is given by

$$\langle \ell_p \rangle = \frac{4}{3} r_p \frac{po}{1 - po} \tag{24}$$

The tortuosity of such systems is

$$\tau = \frac{13}{9} \tag{25}$$

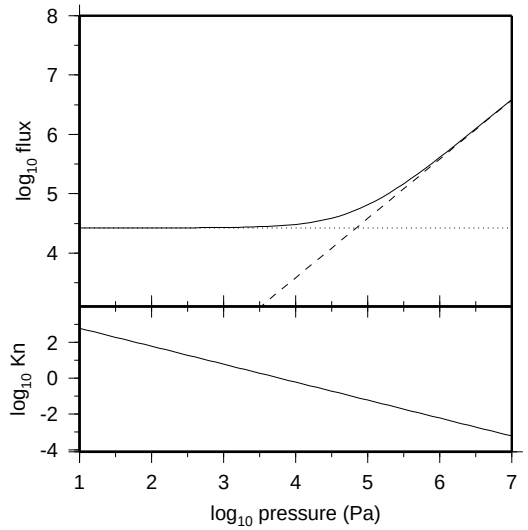

Fig. 1. Diffusion flux (H_2O) of a binary gas mixture across a capillary (diameter 1 μm) at 150 K with constant pressure gradient. The gas is composed of H_2O (50 %) and CO (50 %). The 3 curves are obtained with the Poiseuille (viscous, dashed line) and Knudsen (free molecular, dotted line) formula as well as with the *Chapman-Enskog* method (solid line). For comparison the Knudsen number is plotted below.

We relate a similar geometrical correction to the viscous diffusion coefficient. The parameter ξ of Eq. (15) then becomes

$$\xi = \frac{6}{13\pi r_p^2}\frac{po}{1-po} \tag{26}$$

An additional heat source is taken into account for advection. The gas transports enthalpy and is supposed to thermalise immediately with the solid phase.

$$\dot{H}^{ad} = c_{v,\,i}\frac{m_i}{k_B T}\Delta T\ \nabla\left(D_i^d \nabla p_i + D_i^v \nabla p\right) \tag{27}$$

with the specific heat $c_{v,\,i}$ of species i.

2.4. Boundary conditions and singularities

Each diffusion equation has two boundary conditions per dimension. In our model these equations are solved for two spatial dimensions (r, radius and θ, colatitude) using spherical coordinates. After writing out all terms of these equations there appear singularities at $r = 0, \theta = 0$ and $\theta = \pi$. If the problem is symmetrical with respect to the origin it follows by doing Maclaurin's expansion that the diffusion equation at $r = 0$ becomes

$$\frac{\partial u}{\partial t} = 3\ \frac{\partial^2 u}{\partial r^2} \tag{28}$$

(with $u \equiv T, p$). Fortunately the singularities at $\theta = 0$ and $\theta = \pi$ can be approximated with the de l'Hopital rule

$$\lim_{\theta\to 0,\pi}\frac{1}{\tan\theta}\frac{\partial u}{\partial\theta} = \frac{\partial^2 u}{\partial\theta^2} \tag{29}$$

Each segment of the sphere is treated independently and no flux can pass the inner borders (von Neumann conditions).

$$\left.\frac{\partial T}{\partial r}\right|_{r=0} = 0\,,\ \left.\frac{\partial T}{\partial\theta}\right|_{\theta=0} = 0\,,\ \left.\frac{\partial T}{\partial\theta}\right|_{\theta=\pi} = 0$$

$$\left.\frac{\partial p_i}{\partial r}\right|_{r=0} = 0\,,\ \left.\frac{\partial p_i}{\partial\theta}\right|_{\theta=0} = 0\,,\ \left.\frac{\partial p_i}{\partial\theta}\right|_{\theta=\pi} = 0$$

The last boundary condition has to be determined for each point of the spherical surface (Dirichlet conditions). The received solar flux per unit surface at a given time, corresponding to a declination δ of the Sun and to a heliocentric distance r_h (in AU), is given by

$$S = S_0\left(\frac{1}{r_h}\right)^2\cos z \tag{30}$$

S_0 is the solar constant for 1 AU. The zenith distance of the Sun z is found by using the theorem of spherical triangles.

$$\cos z = \sin\phi\ \sin\delta + \cos\phi\ \cos\delta\ \cos\Omega \tag{31}$$

where ϕ is the latitude and Ω is the hour angle of the considered point. During the night phase ($\cos z < 0$) the direct solar flux is equal to zero and only a small arbitrary background radiation of 20 K due to scattered light in the coma is considered. The declination δ is related to the true longitude of the Sun (λ) by

$$\sin\delta = \sin\lambda\ \sin\varepsilon \tag{32}$$

where ε is the obliquity or the tilt of the nucleus rotation axis relative to the orbital plane. λ is connected to the true anomaly ν by

$$\lambda = \nu + \tilde{\omega} \tag{33}$$

$\tilde{\omega}$ is the true anomaly of the vernal equinox. Let us note that ε and $\tilde{\omega}$ define the orientation of the nucleus rotation axis with respect to the Sun. The comet – Sun distance is given by the ellipse equation.

$$r_h = \frac{a\left(1-e^2\right)}{1+e\cos\nu} \tag{34}$$

The ellipse is defined by its semi-major axis a and its eccentricity e. In the case of P/SW1 $a = 6.04$ AU and $e = 0.045$. The angular velocity of the orbital motion is

$$\dot{\nu} = \frac{1}{r_h^2}\sqrt{GMa\left(1-e^2\right)} \tag{35}$$

where G is the gravitational constant and M is the mass of the Sun.

At surface, the temperature is inferred from the energy balance of a sublimating, conducting layer of finite thickness.

$$S\,(1-Al) = \epsilon\sigma T^4 + L^s_{\mathrm{H_2O}}\dot{Z}_{\mathrm{H_2O}} + K\nabla T + \Delta r\dot{H} \tag{36}$$

where Al is the albedo. $L^s_{\mathrm{H_2O}}$ is the latent heat of sublimating water ice and $\dot{Z}_{\mathrm{H_2O}}$ is the mass loss rate per unit surface.

$$\dot{Z}_{\mathrm{H_2O}} = \alpha\, p^s_{\mathrm{H_2O}}\, \frac{\tilde{\rho}_{\mathrm{H_2O}}}{\tilde{\rho}_{\mathrm{H_2O}} + \tilde{\rho}_d} \sqrt{\frac{m_{\mathrm{H_2O}}}{2\pi k_B T}} \tag{37}$$

Any temperature change will be lessened by the enthalpy change term $\Delta r \dot{H}$. In the model we suppose that in any case there is no condensed CO or amorphous ice present within the surface layer.

The pressure change at surface is

$$\begin{aligned}\frac{\partial p_{\mathrm{H_2O}}}{\partial t} &= \mathscr{S} \cdot \alpha \left(p^s_{\mathrm{H_2O}} - p_{\mathrm{H_2O}}\right) \sqrt{\frac{k_B T}{2\pi m_{\mathrm{H_2O}}}} \\ &+ \nabla \left(D^d_{\mathrm{H_2O}} \nabla p_{\mathrm{H_2O}}\right) + \nabla \left(D^v_{\mathrm{H_2O}} \nabla p\right)\end{aligned} \tag{38}$$

and $0 \le p_{\mathrm{H_2O}} \le p^s_{\mathrm{H_2O}}$. The CO partial pressure at surface is supposed to be zero in the model. This hypothesis holds if no condensed CO is present in the surface layer and the potential effusion is larger than the diffusion flux just below the surface.

3. Discretisation and numerical resolution

The spherical nucleus with the radius R_n is subdivided into concentric shells. The radial depth of the shells increases from surface to centre by an exponentially growing step. Each meridian is cut into N_k pieces unequal in size. The corresponding latitudinal surface belts are chosen so that each belt receives an identical amount of solar flux for a zero obliquity of the nucleus rotation axis. To each belt corresponds the energetically averaged mean latitude

$$\bar{\phi}_k = \mathrm{acos}\left[\frac{\pi}{2N_k}\left(\sin\phi_{k+1} - \sin\phi_k\right)\right] \tag{39}$$

The sphere is divided into segments of equal size. The subvolumes are discretised using a centred spatial grid.

The set of diffusion equations can be solved by applying a finite difference method. An efficient scheme for parallel computing is the *operator splitting method* (e.g. Hockney & Eastwood 1988; Press et al. 1992). The basic idea of this method is to split the time integration step Δt. The diffusion equation, written in operator form,

$$\frac{\partial u}{\partial t} = -\left(\mathscr{L}_r + \mathscr{L}_\theta\right) u + q \tag{40}$$

(with $q \equiv \sum \dot{Q}, \sum \dot{H}$ and the differential operator $\mathscr{L}$) is differenced implicitly in two time steps weighted with the constant value Θ

$$\begin{aligned}\frac{u^{n+1/2} - u^n}{\Delta t/2} &= -\Theta \mathscr{L}_\theta u^{n+1/2} - (1-\Theta)\mathscr{L}_r u^n + q \\ \frac{u^{n+1} - u^{n+1/2}}{\Delta t/2} &= -(1-\Theta)\mathscr{L}_\theta u^{n+1/2} - \Theta \mathscr{L}_r u^{n+1} + q\end{aligned} \tag{41}$$

Rearranging and writing in matrix vector notation, we have

$$\begin{aligned}\left[\mathbf{I} + r\Theta\mathscr{L}_\theta\right]\mathbf{u}^{n+1/2} &= \left[\mathbf{I} - r(1-\Theta)\mathscr{L}_r\right]\mathbf{u}^n + r\mathbf{q} \\ \left[\mathbf{I} + r\Theta\mathscr{L}_r\right]\mathbf{u}^{n+1} &= \left[\mathbf{I} - r(1-\Theta)\mathscr{L}_\theta\right]\mathbf{u}^{n+1/2} + r\mathbf{q}\end{aligned} \tag{42}$$

with $r = \Delta t/2$. $\mathbf{I}$ is a unit matrix. The right hand side can be evaluated readily as it contains only "old" values. The operators on the left hand side of Eq. (42) are tridiagonal matrices that can be solved by applying the Thomas algorithm.

In order to represent derivatives accurately at the boundaries by a central difference formula we used the standard introduction of a fictitious grid point beyond the boundary.

Stability is given for $\Theta \ge 0.5$. We have chosen $\Theta = 0.5$ (*consistent* scheme) for the heat diffusion equation. For large diffusion coefficients very slow decaying finite oscillations can occur between $0.5 \le \Theta < 1$ in the neighbourhood of discontinuities (Smith 1985). To avoid such a case we have chosen $\Theta = 1$ for the gas diffusion equations.

The computation is performed with the message-passing interface MPI (Message-Passing Interface Forum 1995) on a CRAY T3D parallel supercomputer. The used partition has to account for the stepwise integration in the radial and meridional dimensions. We haven chosen a regular domain decomposition for each integration step. After each integration step the entire data matrix is updated by means of a collective communication. One could reduce the number of transferred data by using point to point communications with a structured data type, but, the communication would be more time expensive because of a non-contiguous data access. Various mathematical functions are vetorised by using their corresponding subroutines of the *Benchlib* library. For the given problem size we found the most interesting exploitation with 8 processors. In this configuration the average computation time for one time step is about 50 ms on a CRAY T3D.

4. Physical and numerical parameters

The model nucleus has a uniform temperature of 20 K at the beginning of the simulation so that the condensed CO remains in solid state as its net sublimation rate at this temperature is small in a porous matter. The initial composition has a dust to ice mass ratio of $\psi = 1$ which corresponds to the lower value evaluated for comet 1P/Halley (McDonnell et al. 1991). The ice contains condensed CO with a molar fraction of (free) 10%. An additional amount of 10% is trapped by the amorphous water ice. The compact dust density is assumed with $\rho_d = 3000\,\mathrm{kg\,m^{-3}}$. One single density is chosen for the ice $\rho^c_{\mathrm{H_2O}} = \rho_{\mathrm{H_2O}}{}^a = \rho_{\mathrm{CO}} = 920\,\mathrm{kg\,m^{-3}}$. The initial total mass density is $\rho = 450\,\mathrm{kg\,m^{-3}}$ which is a mean value of Rickman's density estimation for comet 1P/Halley (Rickman 1986). The porosity is $po \approx 0.68$. The material is supposed to be built by accretion of micrometre-sized aggregates. Accordingly, we have chosen a characteristic pore size $r_p = 1\,\mu$m.

The thermal conductivity of compact water ice has been evaluated by Klinger (1980). For crystalline ice he found a T^{-1} dependency by means of laboratory experiments.

$$K^c_{H_2O} = \frac{567}{T} \ \mathrm{W\,m^{-1}\,K^{-1}} \tag{43}$$

For amorphous ice Klinger suggested a very low conductivity derived from the classical phonon model for solids.

$$K^a_{H_2O} = 2.34\,10^{-3}\,T + 2.8\,10^{-2} \quad \mathrm{W\,m^{-1}\,K^{-1}} \tag{44}$$

Recently, Kouchi et al. (1992) have measured values several orders of magnitude lower. An explanation of this huge difference might be a weakly connected structure of the condensed sample. Nevertheless, already Klinger's value is so small that the main contribution to the heat transport should come from the gas phase and is not due to heat conduction. In our model we use Klinger's expression as an upper limit of the contribution of the amorphous ice. The conductivity of condensed CO is expected to be small if the molecules are in the amorphous phase. Therefore we use for CO the same conductivity as for amorphous H_2O. The bulk conductivity of the dust is adopted from the mean conductivity of terrestrial minerals given by Drury et al. (1984).

$$K_d = 2 \ \mathrm{Wm^{-1}K^{-1}} \tag{45}$$

The specific heat of crystalline water ice has been fitted by Klinger (1980) from measured data given by Giauque & Stout (1936).

$$c_{p,H_2O} = 7.49\,T + 90 \quad \mathrm{Jkg^{-1}K^{-1}} \tag{46}$$

The same expression is adopted for amorphous ice. For CO we use the upper limit suggested by Tancredi et al. (1994) although small deviation occurs below $T < 61.55$ K: $c_{p,CO} = 2010$ $\mathrm{Jkg^{-1}K^{-1}}$. The specific heat of the dust is supposed to be:

$$c_{p,d} = 3\,T \quad \mathrm{J\,kg^{-1}\,K^{-1}} \tag{47}$$

This formula fits the specific heat of terrestrial minerals measured at room temperature (Drury et al. 1984). The specific heat of water vapour and CO gas is inferred from the ideal gas law approximation: $c_{v,H_2O} = 3k_B/m_{H_2O}$ and $c_{v,CO} = \frac{5}{2}k_B/m_{CO}$.

The latent heat of sublimation of pure H_2O is given by Cowan & A'Hearn (1979) from a fit of older data (Washburn 1928).

$$L^s_{H_2O} = 1.86\,10^6 - 718\,T \quad \mathrm{J\,kg^{-1}} \tag{48}$$

The lower limit of latent heat of sublimation of volatile molecules condensed in a water ice matrix is estimated from the adsorption energy (Schmitt 1991): $L^s_{CO} = 2.93\,10^5$ $\mathrm{J\,kg^{-1}}$.

The energy balance of the crystallisation process is calculated using the latent heat of crystallisation of pure amorphous water ice of $9\,10^4 \mathrm{J\,kg^{-1}}$ (Ghormley 1968). The energy of evaporation of trapped CO is approximated by its latent heat of sublimation. This description is consistent with the endothermic process observed during the crystallisation of water ice being strongly enriched with CO_2 (Kouchi 1995). For the chosen parameter the threshold amount of trapped CO for an endothermic process is ≈ 23 % (molar). Other works (Prialnik et al. 1992; Tancredi et al. 1994) consider that the trapped CO behaves as a gas and the energy reduction during the gas release is therefore much lower.

The sticking (or condensation) coefficient α (Eq. 38) for H_2O on ice surfaces has been measured by Haynes et al. (1992). α is temperature dependent. After fitting the measured data by a linear law we get

$$\alpha = -2.1 10^{-3}\,T + 1.042 \quad (\text{ with } T > 20 \text{ K}) \tag{49}$$

The saturated vapour pressures are approximated by

$$p^s_i = A_i \exp\left(-B_i/T\right) \tag{50}$$

where $A_{H_2O} = 3.56\,10^{12} \mathrm{N\,m^{-2}}$, $B_{H_2O} = 6141.667$ K (Fanale & Salvail 1984) and $A_{CO} = 1.6624\,10^9 \mathrm{N\,m^{-2}}$, $B_{CO} = 764.16$ K (Fanale & Salvail 1990). More precise formula of the vapour pressure exist (e.g. Washburn 1928, Kouchi 1987). However, taking into account the uncertainties in the description of the sublimation process we have chosen Eq. (50) as it allows more efficient computation.

The nucleus surface is supposed to be dark which is the actual image influenced by the analysis of the optical properties of comet 1P/Halley. It is also consistent with the presence of complex hydrocarbons suggested by Greenberg (1982). We use an albedo of 0.05 and an infrared emissivity of 0.9.

The model nucleus has a spherical shape with a radius of $R_n = 10$ km (see Meech et al. 1993). The nucleus radius is discretised by 2^7 grid points. The first layers under the surface have a thickness of 0.1 m. The deepest layers have a thickness of a few hundred metres. Each meridian contains 2^5 grid points. The nucleus rotation around its spin axis is cut into 2^5 steps leading to a data matrix with the size of 2^{17} elements per rotation.

To resolve the diurnal heat wave the numerical integration time step Δt has to be sufficiently small. But the smaller the time step the larger the computation time for a given problem size. In order to know how good the diurnal heat wave is resolved we compare a characteristic propagation time τ with Δt. The characteristic time can be defined as the ratio of the space resolution to the propagation velocity: $\tau = \Delta r/v$. The propagation velocity of a diffusion wave is

$$v = 2\sqrt{\frac{K}{\rho c_p}\,\frac{\pi}{P}} \tag{51}$$

where P is the nucleus spin period. Using a heat conductivity of $K = 0.1\,\mathrm{W\,m^{-1}\,K^{-1}}$, a mass density of $\rho = 450\,\mathrm{kg\,m^{-3}}$, a

specific heat of $c_p = 1000\,\mathrm{J\,kg^{-1}\,K^{-1}}$ and $P = 10$ days we get with $\Delta r = 0.1$ m a characteristic time scale of $5\,10^4$ seconds. This value is compared to the chosen time step.

$$\frac{\Delta t}{\tau} = \frac{P/N_\Omega}{5\,10^4} \approx 0.5 \tag{52}$$

The integration time step is small compared to the diffusion time scale. A further necessary condition is on the size of the space resolution. Δr should be smaller than a characteristic depth of penetration of the diurnal heat wave. We consider the damping of a harmonic diffusion wave by a factor x (with $x < 1$) at the depth r

$$r = -\sqrt{\frac{K}{c_p\rho}\,\frac{P}{\pi}}\;\cdot\;\ln x \tag{53}$$

For $x = 0.1$ the penetration depth is equal to about $r = 0.57$ m corresponding to 5 layers. One can therefore expect that the diurnal heat wave can be resolved with the chosen time and space resolution.

5. Parametrisation of surface erosion

So far our model description contains only the mass loss due to sublimation and subsequent effusion. Nevertheless emission of solid particles from the surface takes place which can be evaluated by broadband photometry. These grains are dragged out of the ice-dust matrix by the escaping gas. If CO is the most important driver of the activity of P/SW1 there should exist a correlation function $\mathscr{F}$ relating the dust emission rate $\dot{Q}_d$ to the CO gas production rate $\dot{Q}_{\mathrm{CO}}$.

$$\dot{Q}_d = \mathscr{F}\,\dot{Q}_{\mathrm{CO}} \tag{54}$$

A microphysical description of this process is complex and difficult to quantify as the origin of the cohesion forces (physical or chemical) is unknown. Therefore, we have chosen to parametrise $\mathscr{F}$. It seems that $\mathscr{F}$ has the property of an amplification function as the measured CO production rate is more or less constant but the brightness varies several orders of magnitudes. This non-linearity could also be an artefact due to grain fragmentation as the collision rate per unit volume increases with the square of grain density.

At the current state of the model development we prefer to retain a linear relationship between $\dot{Q}_d$ and $\dot{Q}_{\mathrm{CO}}$. We consider a constant normalised grain size distribution. Such a case is favoured with particles having a fractal dimension of $D = 2$ since the density $\rho(r)$ of a fractal decreases in this case with size according to the relation

$$\rho(r) \propto r^{D-3} \tag{55}$$

This fractal dimension is yielded from accretion models of the primordial solar nebula (Meakin & Donn 1988). Finally the parametrisation of the mass loss rate becomes

$$\mathscr{F} = \left.\frac{\dot{Q}_d}{\dot{Q}_{\mathrm{CO}}}\right|_{\mathrm{model}} = \left.\frac{\langle\dot{Q}_d\rangle}{\langle\dot{Q}_{\mathrm{CO}}\rangle}\right|_{\mathrm{observation}} \tag{56}$$

The modelled CO production rate is

$$\dot{Q}_{\mathrm{CO}} = \sum_{N_k}\sum_{N_\Omega} A\,\frac{D^d_{\mathrm{CO}}}{k_B T}\,\left.\frac{\partial p_{\mathrm{CO}}}{\partial r}\right|_{\mathrm{surface}} \tag{57}$$

where A is the size of a surface element of the discretised sphere.

$$A = \frac{2}{N_\Omega}\pi R_n^2\,|\sin\phi_{k+1} - \sin\phi_k| \tag{58}$$

By analysing isophotes of the dust tail of P/SW1, Fulle (1992) suggested a dust production rate of 600 ± 300 kg s^{-1}. The production rate could even be larger as the used IRAS images contain only information on grains of sizes between 5 μm and 2 cm. Fulle concluded that the persistent coma would result of steady activity rather than of overlaps of outburst shells. One can expect that icy-dust grains are emitted from the surface. If we assume a dust to ice mass ratio of about 1 the water ice erosion rate would be $\approx 600 \pm 300$ kg s^{-1}. The modelled H_2O sublimation rate through free surface sublimation at 6 AU is $\dot{Q}_{H_2O} < 10$ kg s^{-1}. However, the icy grains can completely sublimate and contribute to the H_2O production rate. As water is not observed so far in P/SW1 the H_2O production rate has to be in agreement with the detection limit of 10^{28} molecules s^{-1} (Bockelée-Morvan, private communication).

The CO production rate is given by radio spectroscopic observations. The measured CO gas production rate is about 1200 to 2000 kg s^{-1} (Senay & Jewitt 1994; Crovisier et al. 1995). The parameter $\mathscr{F}$, relating the dust and CO gas production rate, is therefore chosen equal to 0.5 .

Although the erosion is not strictly uniform we suppose that the approximation of the spherical shape of the model nucleus holds for the simulation over a few revolutions.

6. Results and discussion

Comet 29P/Schwassmann-Wachmann 1 is of particular interest for a better understanding of physico-chemical processes and composition inside a comet nucleus. Compared to other short period comets its activity is *a priori* not dominated by sublimation of water ice. Furthermore, due to small CO photodissociation rates at a heliocentric distance of 6 AU the photochemistry is straightforward.

The results presented and discussed in this work are restricted to a small set of input parameters. The response of the model depends obviously on the choice of these parameters. We have chosen to take special attention to the tilt of the nucleus spin axis, the amorphous-crystalline phase transition and the surface erosion. We have considered the cases of an obliquity $\varepsilon = 0°$ and $\varepsilon = 90°$, an initial composition with and without amorphous ice, as well as the two cases where no surface erosion is taking place or a parametrised erosion rate.

In this work we used a constant value $h = 0.1$ for the parametrisation of the hertz factor (Eq. 13). Furthermore we adopted a true anomaly of the vernal equinox of $\tilde{\omega} = 90°$ to obtain a maximal seasonal difference (Eq. 33).

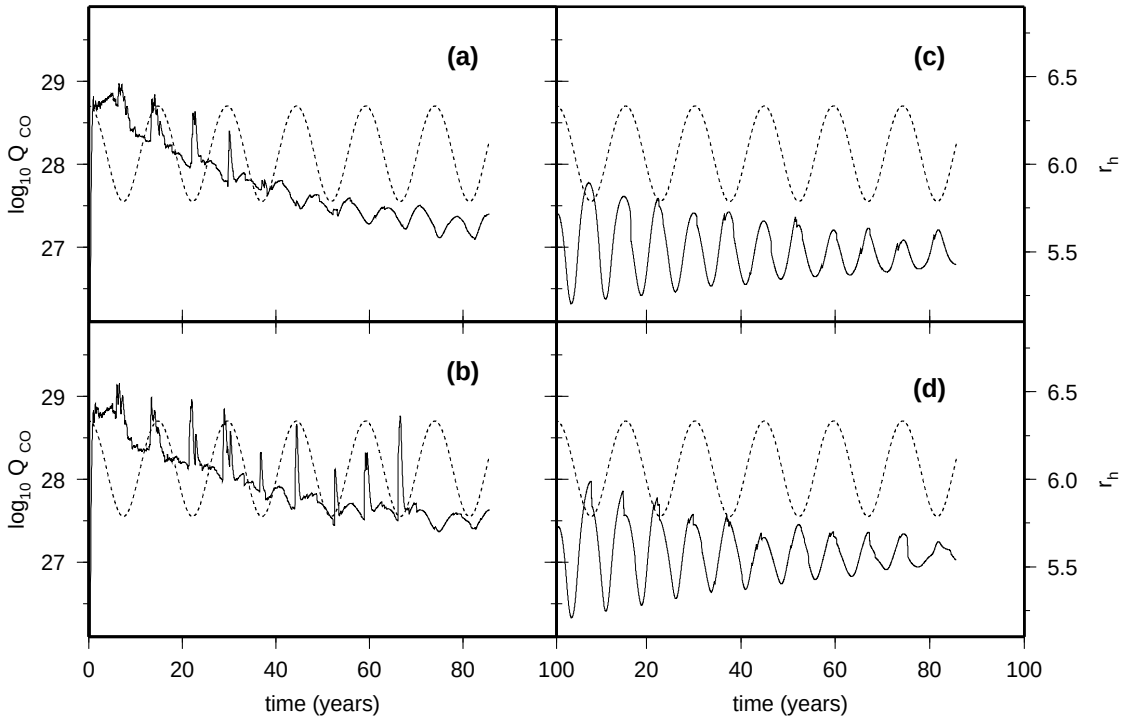

Fig. 2a–d. CO gas production rates in molecules s^{-1} (full line) with respect to time for an obliquity of 90° and heliocentric distance r_h in AU (dashed line) is plotted for each configuration: **a** initially amorphous ice, no surface erosion; **b** initially amorphous ice, with surface erosion (see Eq. 56); **c** initially crystalline ice, no surface erosion; **d** initially crystalline ice, with surface erosion.

Fig. 2a–d shows the CO production rates in molecules s^{-1} with respect to time for a nucleus having its spin axis in its orbital plane ($\varepsilon = 90°$). In the case of an initial amorphous composition the CO production rate is about $5\,10^{28}$ molecules s^{-1}. If no erosion is taken into account (a) $\dot{Q}_{\rm CO}$ decreases regularly to about $2\,10^{27}$ molecules s^{-1} after 6 revolutions. The penetrating heat wave induces crystallisation within the first metre below the surface. During strong crystallisation $\dot{Q}_{\rm CO}$ increases by about a factor 3. Small outbursts are hidden by the continuous activity due to sublimation of condensed CO. If no erosion occurs the amorphous ice front becomes rapidly too deep to be heated above a critical temperature which would induce crystallisation. The activity is different if the surface layer is eroded (b) continuously as a function of the CO outflow ($\mathscr{F} = 0.5$, see Eq. 56). The choice of the correlation function determines if an outburst regime is maintained or not. If no amorphous ice is initially in the ice-dust matrix (case c and d) the CO gas production is about one order of magnitude smaller than in the previous case. This behaviour is explained by the low thermal conductivity of amorphous water ice. Since the conductivity of crystalline ice is several orders of magnitude larger, more heat is conducted to deeper layers so that local heating is prevented. Due to the low CO production rate the dust emission and surface erosion is also weak so that the case without erosion (c) is similar to the case with a parametrised surface erosion (d). We note that $\dot{Q}_{\rm CO}$ is strongly correlated with the apsides in all 4 cases (a-d). The heat diffusion into the nucleus requires a certain time before the heat wave reaches the sublimation front (a,b). This delay is seen with respect to the heliocentric distance. In the case (c) and (d) the CO sublimation front is still close to the surface after 6 revolutions as the CO mass loss is small. Such a behaviour has also been noted for the observed lightcurve of P/SW1 (Cabot et al. 1996).

The surface is approximately uniformly eroded. After 6 revolutions the volume corresponding to 0.2 m depth or 2 entire layers have been lost at each latitude (b). The local activity averaged over one revolution is thus more or less comparable for the different surface elements. From this volume loss we can evaluate the average dust production of $\dot{Q}_d \approx 20$ kg s^{-1}. For a better fit of the observation more surface material has to be eroded.

Fig. 3e–h shows the CO production rates with respect to time for a nucleus having its spin axis perpendicular to its orbital plane ($\varepsilon = 0°$). In none of the studied cases crystallisation occurred as the heating periods are too short to obtain sufficiently high temperatures below surface. The CO production rates are again larger for the cases of amorphous ice: no erosion (e), with erosion (f). If no erosion occurs then the production rate is slowly decreasing. In the other case where the CO drags out ice-dust grains the CO production rate is larger because of the continuous surface erosion. $\dot{Q}_{\rm CO}$ is smaller if only crystalline water ice is considered: no erosion (g), with erosion (h). The reason is the same as the one given above. In these cases appear a correlation between $\dot{Q}_{\rm CO}$ and heliocentric distance.

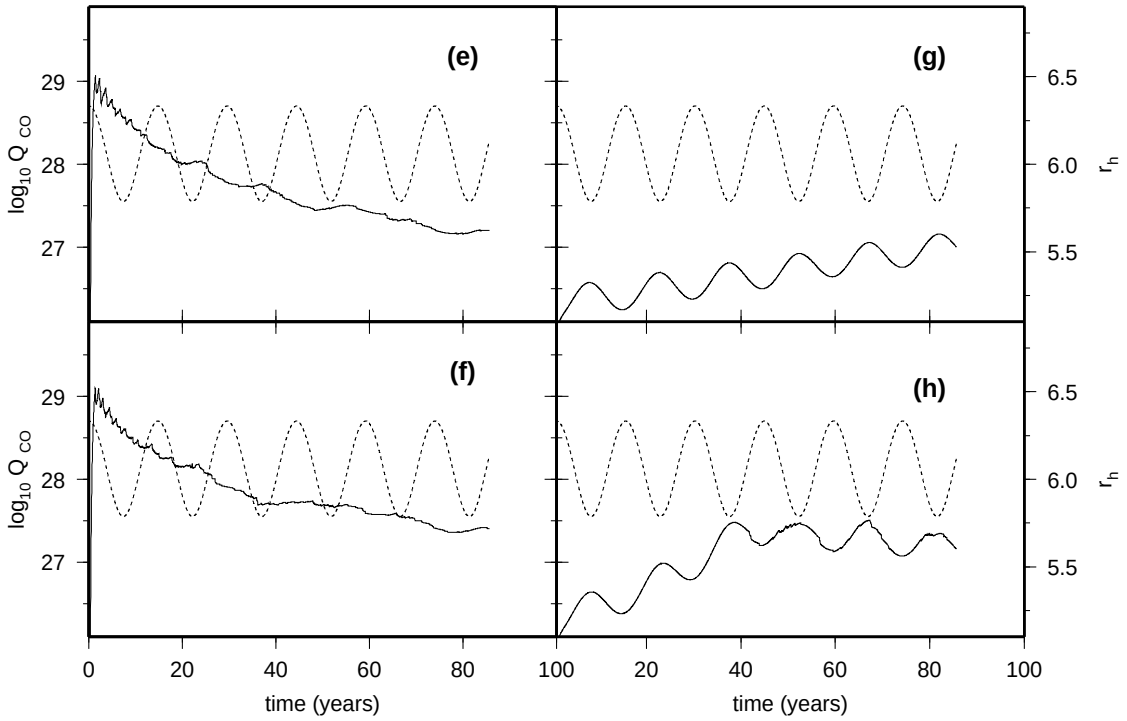

Fig. 3e–h. CO gas production rates (full line) with respect to time for an obliquity of 0° and heliocentric distance r_h in AU (dashed line) is plotted for each configuration: **e** initially amorphous ice, no surface erosion; **f** initially amorphous ice, with surface erosion (see Eq. 56); **g** initially crystalline ice, no surface erosion; **h** initially crystalline ice, with surface erosion.

Fig. 4a and b shows the CO molar concentration after 6 revolutions (only free CO, no trapped CO) within the nucleus. Due to the CO mass loss the sublimation front penetrates into the interior. We have found that the stronger the sublimation at a given region within the nucleus, the stronger the recondensation in the deeper neighbouring layers.

Fig. 5 shows the molar concentration of amorphous ice after 6 revolutions for case (a). The crystallisation takes places in the polar regions where the highest surface temperatures are obtained.

The model results are rather different for the diverse chosen configurations. The results of configuration (b) with an obliquity of $\varepsilon = 90°$, an initial amorphous ice composition and a parametrised grains emission fits the best the observations. The CO gas production rate is initially about $5\,10^{28}$ molecules s^{-1}, sudden peaks during a short period of time and the correlation with the apsides correspond to the observed features. None of them is found if only crystalline ice is considered. Nevertheless a comparable CO gas production rate could be obtained for crystalline ice for an initially extremely low hertz factor which may increase close to surface due to grain sintering. But for this case we would need another cause to explain the sudden release of CO during an outburst.

Fig. 6 shows the surface temperature at a pole and at the equator for the configuration (a). In this case the simulated temperatures at both poles vary from 155 K and 150 K during the period of maximal insolation to about 40 K at the antipode. No direct measurement of the nucleus surface temperature exists. However, the coma expansion velocity can be derived from the Doppler shift of a radio line in the spectroscopic signal. Following Crovisier et al. (1995) the coma expansion velocity on the day side of P/SW1 is $v = 480\,\mathrm{m\,s^{-1}}$ and $v = 300\,\mathrm{m\,s^{-1}}$ on the night side. The energy balance of a CO dominated coma without any photochemical processes is

$$e_{\mathrm{tot}} = e_{\mathrm{trans}} + e_q \tag{59}$$

$$\frac{5}{2}k_B T_n = \frac{1}{2}m_{\mathrm{CO}}v^2 + e_q \tag{60}$$

where e_{tot} is the enthalpy (without rotational energy) of the gas at surface and e_{trans} is the translational energy. e_q represents energy sinks like the energy transfer to solid particles. Since collisions are not so efficient in producing rotational cooling as for translational cooling the adiabatic cooling following the coma expansion is more important than the rotational cooling. Therefore the energy balance can be written without the terms for rotational energy. As the grains are only weakly coupled to the gas coma we adopt $e_q \approx 0$. The nucleus surface temperature T_n corresponds to the effusion temperature if the gas is completely thermalised. After computation of Eq. (60) we obtain temperatures $\approx$ 156 K on the day side and $\approx$ 61 K the night side respectively. These temperatures are significantly higher than those suggested (100 K and 40 K) from an analogue H_2O coma by Crovisier et al. (1995). The high temperature on the day

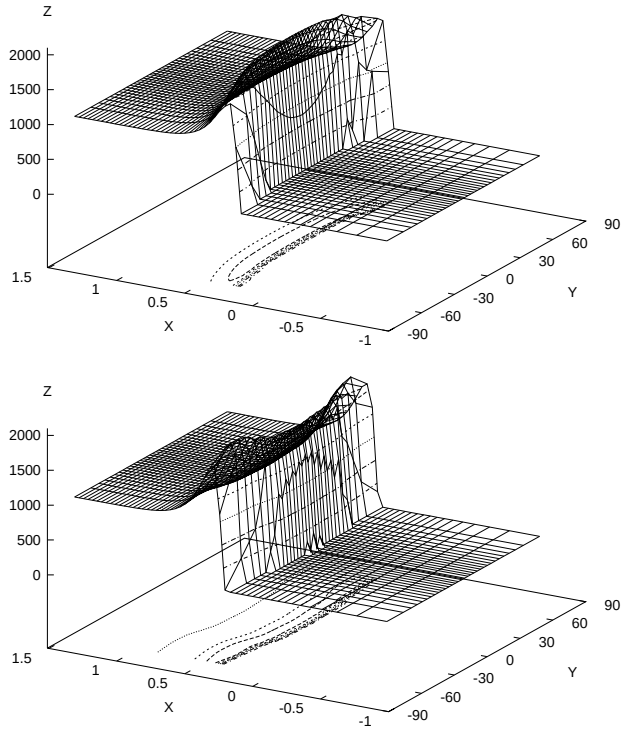

Fig. 4a and b. CO molar concentration within the first few metres below surface after 6 revolutions. Top: obliquity 90° (**a**), bottom: obliquity 0° (**b**). $X \mathrel{\widehat{=}} \log_{10}$ depth (metre), $Y \mathrel{\widehat{=}}$ latitude (°) and $Z \mathrel{\widehat{=}}$ molar concentration (moles m^{-3}).

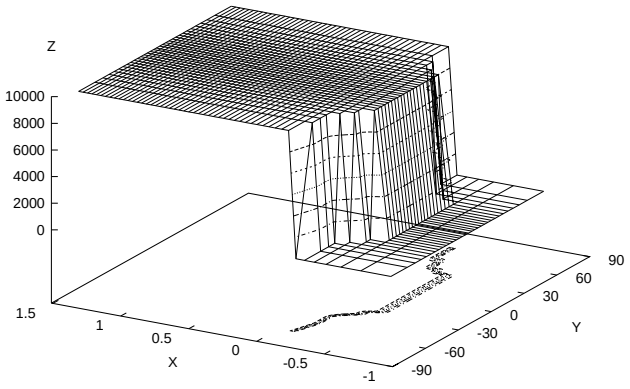

Fig. 5. Molar concentration of amorphous ice within the first few metres below surface after 6 revolutions. Plotted only for configuration (a). $X \mathrel{\widehat{=}} \log_{10}$ depth (metre), $Y \mathrel{\widehat{=}}$ latitude (°) and $Z \mathrel{\widehat{=}}$ molar concentration (moles m^{-3}).

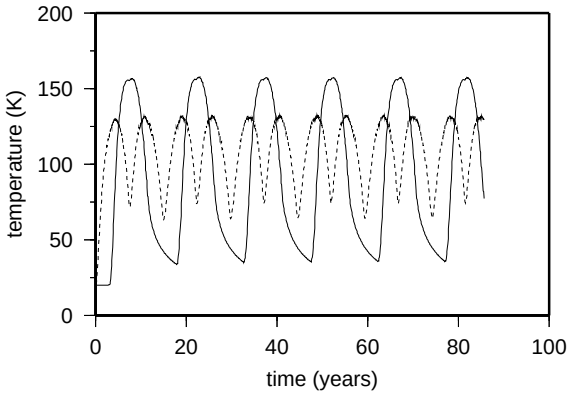

Fig. 6. Maximal surface temperatures for a nucleus with an obliquity 90° (a), plotted for the pole directed to the Sun at perihelion (full line) and the equator (dashed line).

side is consistent with the black body temperature at 6 AU. The day side temperature corresponds quite well to our model result for a inclined spin axis, but so does not the night temperature. A better fit would be obtained for an intermediate obliquity.

The results of the presented simulation are an important clue for the presence of amorphous ice in comets. Amorphous ice is observed in molecular clouds (see Léger et al. 1979) and suspected to exist in comets. It has been proposed by Haruyama et al. (1993) and Prialnik & Podolak (1995) that a nucleus containing amorphous water ice and minerals could have completely crystallised as a result of radiogenic heating during its stay in the Oort cloud in case of a very low thermal conductivity. Nevertheless the result could be different if one assumes the presence of volatiles which reduce any local temperature increase by the latent heat of sublimation and a larger effective thermal conductivity.

A final remark concerns the nucleus spin period. The chosen period of P = 10 days has the advantage to allow a larger numerical integration step Δt but could be too large compared to the real rotation period which is unknown so far. A recent estimation by Meech et al. (1993) comes up with periods of 14 and 32 hours depending on the rotational state. However, our results would not be very different as in the case of maximal tilt of the nucleus spin axis ($\varepsilon = 90°$) the period plays only a minor role. For $\varepsilon = 0°$ the crystallisation of amorphous ice would even be less likely. The maximal surface temperatures would be lower as the heat wave through heat conduction propagates roughly proportional to $\sqrt{1/P}$. However using a much lower hertz factor crystallisation could occur.

7. Conclusions

The activity of comet 29P/Schwassmann-Wachmann 1 has been studied by means of numerical modelling. A comet nucleus model with a 3D space resolution and an improved description of the gas diffusion has been developed. The model takes into account the phase changes due to crystallisation and sublimation of volatile species inside a porous nucleus composed of ices and dust. The received solar heat flux generates heat and gas diffusion which is simulated in both radial and meridional directions. A 3D solution is obtained by gathering a set of 2D solutions whose boundary conditions depend on the third space dimension (hour angle). The gas diffusion coefficients

are determined using the *Chapman-Enskog* method (Chapman & Cowling 1960).

Various configurations have been assumed and simulated. Special attention was taken to the tilt of the nucleus spin axis. An initial amorphous ice composition and surface erosion was considered. Several important conclusions can be made on the basis of the model results:

1. The orientation of the nucleus rotation axis of P/SW1 is very important for the thermodynamic evolution of the nucleus. Outbursts are more likely for an obliquity of $\varepsilon = 90°$ than for an obliquity of $\varepsilon = 0°$. Furthermore, the CO gas production rates are correlated with the apsides. This behaviour is in good agreement with the results of an independent data analysis published by Cabot et al. (1996).
2. Erosion of surface material seems to be necessary to keep amorphous water ice close to the surface. Only in the case where $\varepsilon = 90°$ outbursts have been found along all 6 revolutions. A dust erosion rate of a few hundred kilogramme per second is likely to maintain an outburst regime if the dust to ice mass ratio is about 1. This erosion rate is in agreement with the observed dust production rate given by Fulle (1992).
3. The range of the modelled CO gas production rates is consistent with the measured production rates of about 10^{28} molecules s^{-1}. The CO sublimation front can be expected within the first 10 metres below the surface. If no surface material is eroded, the activity decreases continuously.

These results give an important hint for the presence of amorphous water ice in cometary nuclei. The crystallisation of amorphous water ice and the release of trapped gases can account for outbursts. This explanation is compatible with the interpretation of comet Halley's outburst in 1991 at 14 AU (see Schmitt et al. 1991; Prialnik & Bar-Nun 1992).

Acknowledgements. A.Enzian would like to thank the members of the Edinburgh Parallel Computing Centre for their hospitality during a research visit funded by the European Union (programme *Human Capital and Mobility*). Many useful suggestions from G. Smith led to an improvement of the parallelisation of the model. The computation of this work were performed on the CRAY T3D of the Institut du Développement des Ressources en Informatique Scientifique (Orsay/France) of CNRS. Part of this work was supported by the French *Programme National de Planétologie* and the Centre National d'Etudes Spatiales. The authors acknowledge useful comments from the referee Dr. G. Tancredi.

References

Benkhoff, J., Huebner, W. F., 1995, Icarus 114, 348
Bouziani, N., 1995, Doctoral thesis, Université Joseph Fourier, Grenoble I
Cabot, H., 1996, Doctoral thesis, Université Joseph Fourier, Grenoble I
Cabot, H., Enzian, A., Klinger, J., Majolet, S., 1996, Planet. Space Sci., in press
Chapman, S., Cowling, T. G., 1960, The Mathematical Theory of Non-Uniform Gases, Cambridge University Press, London
Cowan, J. J., A'Hearn, M. F., 1979, Moon and Planets 21, 155
Crovisier, J., Biver, N., Bockelée-Morvan, et al., 1995, Icarus 115, 213
Drury, M. J., Allen, V. S., Jessop, A. M., 1984, Tectonophysics 103, 321
Dullien, F. A., 1992, Porous Media: Fluid Transport and Pore Structure, Academic Press, New York
Espinasse, S., Klinger, J., Ritz, C., Schmitt, B., 1989, In: J. Hunt, T. D. Guyenne (eds.) Physics and Mechanics of Cometary Materials. Noordwijk, The Netherlands: ESA SP-302, p. 185
Espinasse, S., Klinger, J., Ritz, C., Schmitt, B., 1991, Icarus 92, 350
Fanale, F. P., Salvail, J. R., 1984, Icarus 60, 476
Fanale, F. P., Salvail, J. R., 1990, Icarus 84, 403
Fulle, M., 1992, Nat 359, 42
Ghormly, J. A., 1968, J. Chem. Phys. 48, 503
Giauque, W. F., Stout, J. W., 1936, J. Am. Chem. Soc. 58, 1144
Greenberg, J. M., 1982, In: L. L. Wilkening (ed.) Comets, 131, University of Arizona Press, Tucson
Haruyama, J., Yamamoto, T., Mitzutani, H., Greenberg, J. M., 1993, J. Geophys. Res. (Planets) 98E, 15079
Haynes, D. R., Tro, N. J., George, S. M., 1992, J. Phys. Chem. 96, 8502
Hockney, R. W., Eastwood, J. W., 1985, Computer Simulation using Particles, Adam Hilger, Bristol
Message-Passing Interface Forum, 1995, MPI: A Message Passing Interface Standard, University of Tennessee, Knoxville
Klinger, J., 1980, Science 209, 271
Kömle, N. I., Steiner, G., Seidensticker, K. L., et al., 1992, Planet. Space Sci. 40, 1311
Kouchi, A., 1987, Nat 330, 550
Kouchi, A., Greenberg, J. M., Yamamoto, T., et al., 1992, ApJ 388, L73
Kouchi, A., 1995, In: M. Festou, C. de Bergh, B. Schmitt (eds.) Symposium on Solar System Ices, Toulouse
Léger, A., Klein, J., de Cheveigne, S., et al., 1979, A&A 79, 256
Levitz, P., 1993, J. Phys. Chem. 97, 3813
McDonnell, J. A. M., Lamy, P. L., Pankiewicz, G. S., 1991, In: R. L. Newburn Jr., M. Neugebauer, J. Rahe (eds.) Comets in the Post-Halley Era. Vol. 2, 1043, Kluwer Academic Publishers, Dordrecht
Meakin, P., Donn, B., 1988, ApJ 329, L39
Meech, K. J., Belton, M. J. S., Mueller, B. E. A., et al., 1993, AJ 106, 1222
Present, R. D., 1958, Kinetic Theory of Gases, McGraw-Hill, New York
Press, W. H., Teukolsky, S. A., Vetterling, W. T., et al., 1992, Numerical Recipies, Cambridge University Press, London
Prialnik, D., Bar-Nun, A., 1990, ApJ 363, 274
Prialnik, D., Bar-Nun, A., 1992, In: W. F. Huebner, H. U. Keller, D. Jewitt, et al., (eds.) Workshop on the activity of distant comets. Southwest Research Institute, San Antonio, p. 100
Prialnik, D., Podolak, M., 1995, Icarus 117, 420
Rickman, H., 1986, In: C. Melita (ed.) Comet Nucleus Sample Return Mission. Noordwijk, The Netherlands: ESA SP-249, p. 195
Schmitt, B., 1991, In: D. Benest, C. Froeschle (eds.) Interrelations between Physics and Dynamics for Minor Bodies in the Solar System. Editions Frontières, Paris, p. 256
Schmitt, B., Espinasse, S., Grim, R. J. A., et al., 1989, In: J. Hunt, T. D. Guyenne (eds.) Physics and Mechanics of Cometary Materials. Noordwijk, The Netherlands: ESA SP-302, p. 65

Schmitt, B., Espinasse, S., Klinger, J., 1991, In: A. W. Harris, E. Bowell (ed.) Symposium on Asteroids, Comests and Meteors, Lunar and Planetary Institute, Houston
Senay, M. C., Jewitt, D., 1994, Nat 371, 229
Smith, G. D., 1985, Numerical Solutions of Partial Differential Equations: Finite Difference Methods, Oxford University Press, Oxford
Steiner, G., 1991, Doctoral thesis, Space Research Institute of the Austrian Academy of Sciences, Graz
Tancredi, G., Rickman, H., Greenberg, J. M., 1994, A&A 286, 659
Washburn, E., 1928, International Critical Tables, Vol. 3, p. 210
Whipple, F., 1980, ApJ 85, 305

This article was processed by the author using Springer-Verlag LaTeX A&A style file *L-AA* version 3.